Designable 3D Microshapes Fabricated at the Intersection of Structured Flow and Optical Fields

Rodger Yuan, Maxwell B. Nagarajan, Jaemyon Lee, Joel Voldman, Patrick S. Doyle,* and Yoel Fink*

3D structures with complex geometric features at the microscale, such as microparticles and microfibers, have promising applications in biomedical engineering, self-assembly, and photonics. Fabrication of complex 3D microshapes at scale poses a unique challenge; high-resolution methods such as two-photon-polymerization have print speeds too low for high-throughput production, while top-down approaches for bulk processing using microfabricated template molds have limited control of microstructure geometries over multiple axes. Here, a method for microshape fabrication is presented that combines a thermally drawn transparent fiber template with a masked UV-photopolymerization approach to enable biaxial control of microshape fabrication. Using this approach, high-resolution production of complex microshapes not producible using alternative methods is demonstrated, such as octahedrons, dreidels, and axially asymmetric fibers, at throughputs as high as 825 structures/minute. Finally, the fiber template is functionalized with conductive electrodes to enable hierarchical subparticle localization using dielectrophoretic forces.

The 3D geometric shape of microscale objects has a significant effect on their interactions with the surrounding environment. Nonspherical particles and fibers demonstrate unique properties and are being actively investigated for a wide array

R. Yuan, Prof. Y. Fink
Department of Materials Science and Engineering
Massachusetts Institute of Technology
Cambridge, MA 02139, USA
E-mail: yoel@mit.edu
M. B. Nagarajan, Prof. P. S. Doyle
Department of Chemical Engineering
Massachusetts Institute of Technology
Cambridge, MA 02139, USA
E-mail: pdoyle@mit.edu
J. Lee, Prof. J. Voldman
Department of Electrical Engineering and Computer Science
Massachusetts Institute of Technology
Cambridge, MA 02139, USA
J. Lee, Prof. J. Voldman
Research Laboratory of Electronics
Massachusetts Institute of Technology
Cambridge, MA 02139, USA
Prof. Y. Fink
Microsystems Technology Laboratories
Massachusetts Institute of Technology
Cambridge, MA 02139, USA

The ORCID identification number(s) for the author(s) of this article can be found under https://doi.org/10.1002/smll.201803585.

of applications, including drug delivery, tissue engineering, self-assembly, and photonics. For example, the shape of hydrogel particles has been shown to affect particle–cell interactions[1–3] and the cross-sectional shape of microfibers changes the wicking properties of woven fabrics.[4] In addition, microobjects in nature often take on a nonequilibrium structure to exploit beneficial shape-induced functionality, such as the biconcave geometry of the red blood cell and the triangular cross-section of Saharan silver ant fibers.[5]

Existing techniques to fabricate microobjects with 3D architectures have trade-offs between throughput and shape selection. Conventional layer-by-layer 3D printing techniques based on fused deposition modelling and stereolithography are resolution-limited, with minimum linear feature sizes of over 45 μm.[6] High-resolution 3D printing methods, such as two-photon polymerization, can produce feature sizes as low as 40 nm, but their low print speed makes them unfeasible for production at scale[7] and their small build volumes are unsuitable for fabricating high aspect ratio microobjects such as fibers. Top-down approaches to particle fabrication, such as PRINT[8] and SEAL,[9] are high throughput, but cannot produce 3D shapes beyond stacked 2D extrusions because they utilize polymeric molds of microfabricated templates.

Microfluidic approaches to nonequilibrium particle and fiber synthesis also have a limited library of possible 3D geometries. Droplet-based approaches to nonspherical particle fabrication are restricted to creating particles with equilibrium surface features because the factors that determine the shape of the interface between immiscible fluids are surface tension dominated.[10–14] While flow-lithography based particle fabrication, in which photocurable polymers are flowed through a microfluidic chip and polymerized by UV light passing through a photomask, has shown to have excellent control of particle shape along a single 2D extrusion axis,[15–17] a similar level of shape control in the direction of flow is yet to be achieved.[18–20] In recent years, there have been efforts to improve the complexity of particles beyond 2D extruded shapes through techniques such as hydrodynamic flow shaping[21–23] and nonuniform flow lithography.[24,25] However, the mechanisms enabling these methods, or inertial focusing and nonuniform UV light intensity, are not precise and are difficult to control, limiting particle shape design freedom.

Similarly, microfluidic methods of fiber synthesis rely on methods of shaping microfabricated channel cross-sections that greatly restrict the possible range of cross-sectional shapes. Existing methods of microfluidic fiber synthesis typically utilize capillary tubes,[26–29] which restrict fiber geometry to cylindrical shapes, or polydimethylsiloxane (PDMS) templates built from microfabricated molds,[30,31] which can only produce fiber cross-sections with shapes that can be acid etched from silicon substrates. Hydrodynamic approaches have expanded the range of producible hydrogel fiber cross-sections[32–34] with feature sizes at the sub-micrometer level,[35] but they are not suited for deterministic cross-sectional shape design and lack precise control of fiber shape. Finally, because these techniques are fundamentally based on extrusion, while compositional asymmetry has been demonstrated in fibers along the fiber axis,[27,31] geometric asymmetry along the fiber axis is not easily realizable.

Here, we present a high-throughput and versatile approach to the fabrication of scalable microobjects that significantly broadens the library of manufacturable geometries. Our method is enabled by the thermal drawing process, which uses dimensional reduction to create a uniaxial template with arbitrary cross-sectional features and micrometer resolution.[36–39] Using these hollow fiber templates, we demonstrate biaxial control of the geometries of photopolymerizable hydrogel microparticles, allowing for the logical design and high-throughput synthesis of complex shapes, such as octahedrons and square pyramids. Exposing large areas of the hollow fiber templates to UV light enables microfibers with complex cross-sections and axially asymmetric geometries to be realized. In addition, functionalization of the interior channel walls with conductive materials enables external fields to be produced within the prepolymer flow, allowing for tailored electrokinetic manipulation of subparticles within the hydrogel.

Hollow fiber templates are fabricated using the thermal drawing process, in which an up-scaled version of fiber, called a preform, is heated and drawn into fiber while maintaining its cross-sectional geometry (**Figure 1**a). Complex channel geometries are introduced into the preform via molding of a thermoplastic cladding material around a rigid insert in the shape of the desired channel. Following the molding step, the insert is removed and the preform is drawn into the hollow fiber templates. Because the thermal drawing process utilizes dimensional reduction to achieve sub-millimeter channel sizes, several hundred meters of fiber can be drawn from a single 15 cm preform. This method allows for the fabrication of a hollow channel of any cross-sectional shape, with previous studies demonstrating feature resolution at the micrometer scale.[36]

A wide range of microobjects can be fabricated using the hollow fiber template with various methods of UV-exposure; exposure through a shaped photomask allows for the creation of any microparticle that can be formed by the intersection of two prisms, while large area exposure leads to the formation of hydrogel microfibers with arbitrary cross-section (Figure 1b).

A critical aspect of the hollow fiber templates are the physical properties of the cladding material. We chose cyclic olefin copolymer (COC) as the cladding material for the hollow fiber templates because it had the best combination of high UV transmission and low surface energy. Additional details about the materials selection can be found in the Supporting Information.

High-throughput complex particle fabrication using hollow fiber templates is enabled by three principle components: 1) a hollow fiber template, 2) a photomasked UV beam, and
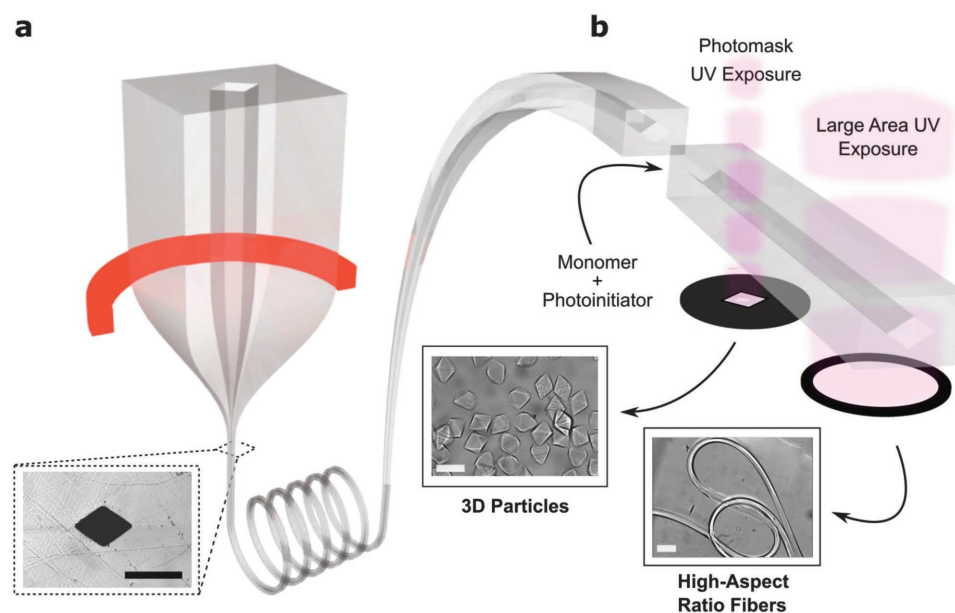

Figure 1. Hollow fiber template microobject fabrication. a) A preform is heated within a furnace (red) and drawn into a fiber. The portion of preform is heated to above its glass transition temperature within the furnace and subjected to a high tensile force in the axial direction, resulting in axial lengthening and transverse dimensional reduction without changing cross-sectional geometry. The preform is mounted to a downfeed to ensure zero net volume flow through the furnace. Inset: A micrograph of a drawn diamond shaped preform. b) After drawing, a solution of monomer and photoinitiator is introduced to a section of the fiber. Based on the method of pulsed UV exposure, it is possible to fabricate complex 3D particles (UV exposure through a photomask) and high aspect ratio hydrogel fibers (large area UV exposure). All scale bars represent 100 μm.
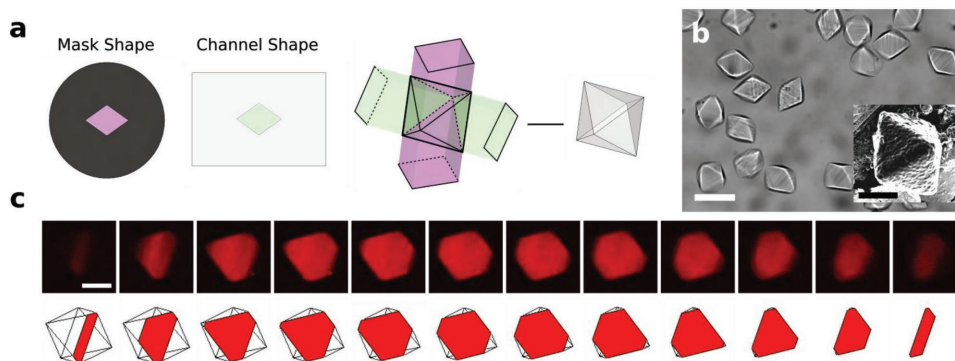
**ADVANCED
SCIENCE NEWS**

www.advancedsciencenews.com

NANO · MICRO

small

www.small-journal.com

Figure 2. Complex 3D microparticle characterization. a) The final shape of a 3D microparticle is determined by the intersection shape between the channel geometry and UV exposure photomask. For example, a mask shape and channel shape comprised of rhombuses with 70.5° acute angles will intersect to create an octahedron. b) Optical image of a cluster of octahedron particles (scale bar 100 µm) with (inset) an SEM image of a single octahedron particle (scale bar 30 µm). c) (Top) Confocal microscopy slices of a single octahedron shaped particle (scale bar 50 µm) with (bottom) corresponding slices of an octahedron shaped particle rendered using CAD software.

3) a digital compressed-air source. We flowed a monomer solution of polyethylene glycol diacrylate (PEG-DA) with photoinitiator (2-hydroxy-2-methylpropiophenone), porogen (PEG), and buffer (1×Tris-Ethylenediaminetetraacetic acid (EDTA)) through the hollow fiber template and positioned the flow perpendicular to the photomasked UV beam. A detailed description of the rationale behind choosing this microobject material can be found in the Supporting Information. When the UV beam is switched on (100–200 ms), only the exposed prepolymer resin is cross-linked into a hydrogel, resulting in a 3D complex particle with biaxial geometric control. We utilized a stop-flow-lithography (SFL) setup, as described in earlier works,[40] in which a compressed air source is connected to a digital 3-way valve to allow for automated flow stopping, polymerization, and restarting of flow. Using this setup, we were able to fabricate particles with diameters as small as 50 µm and at speeds for as high as 825 particles min⁻¹ for a single fiber template with a mask that produces 11 particles per exposure (Video S1, Supporting Information).

We utilize our hollow fiber templating technique to fabricate, to our knowledge, the first reported nonequilibrium octahedron-shaped microparticle. The octahedron particle was fabricated by using rhombus-shaped channels and photomasks (**Figure 2**a) with a maximum end-to-end dimension of 100 µm. We confirmed the octahedral shape of the particle using optical microscopy, scanning electron microscopy (SEM) images of air-dried particles (Figure 2b), as well as confocal microscopy of fluorescently dyed particles in water (Figure 2c).

We utilized the hollow fiber templating to fabricate eight designed particle shapes that have not been reported in literature, including simple geometries such as square pyramids and more complex shapes, like the dreidel, that incorporate both round and sharp edges (**Figure 3**a). The maximum end-to-end dimension of each of the eight fabricated particles was designed to be 100 µm. However, our method allows for minimum free-standing feature thicknesses of as low as 20 µm, as shown in the lip of the picnic table particle and the trusses of the bridge particle. The ability to fabricate complex hydrogel microcomponents with increased degrees of freedom and precision enables the deterministic design of practical particle systems for tailored applications. We demonstrate this by

fabricating a socket-like connector for the dumbbell particle that creates a ball and socket joint system when the corresponding shapes are mixed and agitated within the same container until the dumbbell can randomly connect to the socket (Figure 3b).

Using a large area UV collimated light source, the entire volume of prepolymer solution within the fiber can be polymerized to form a hydrogel fiber. Much like existing hydrogel fabrication methods, hydrogel fiber fabrication in literature is geometrically limited by commercially available capillary tube shapes[26,28] and what can be microfabricated into PDMS chips.[27,30] By contrast, the thermally drawn fiber template allows for complete design freedom in the cross-sectional shape. Furthermore, many existing methods for hydrogel fiber fabrication involve gelation of a resin through interaction with a divalent cation solution.[28,30] These methods are unsuitable for high resolution production hydrogel fibers with complex shapes because the two-phase interface between the resin and the divalent cation solution leads to rounded edges due to surface tension minimization. The polymerization of the hydrogel is a fabrication method that occurs while the prepolymer solution resides inside the template, resulting in high precision fabrication of hydrogels with arbitrary cross-section.

We constructed 3D complex microfibers by removing the photomask and shining UV light over a larger fiber area using an in-house contact lithography setup with a 25 mm UV LED.[41] The hollow fiber template was filled with resin with the same composition as used for the hydrogel particles and a 25 mm section of the template was polymerized using the UV light. **Figure 4**a shows fibers made in diamond shaped, cross shaped, and dumbbell shaped hollow fiber templates, with the cross-section of the fibers shown in the figure insets.

By using high aspect ratio photomasks with identical tip geometries, we were also able to fabricate fibers that, in contrast to typical extrusion methods, demonstrate axial asymmetry. This is possible because the high aspect ratio of hollow fiber template is able to guide a polymerized particle predictably along the flow path. Thus, the high aspect ratio particle can be exposed, translated, and exposed again to create hydrogel fibers with a repeating axial pattern (Figure 4b). Using this technique, we fabricated a hydrogel fiber with alternating lobed
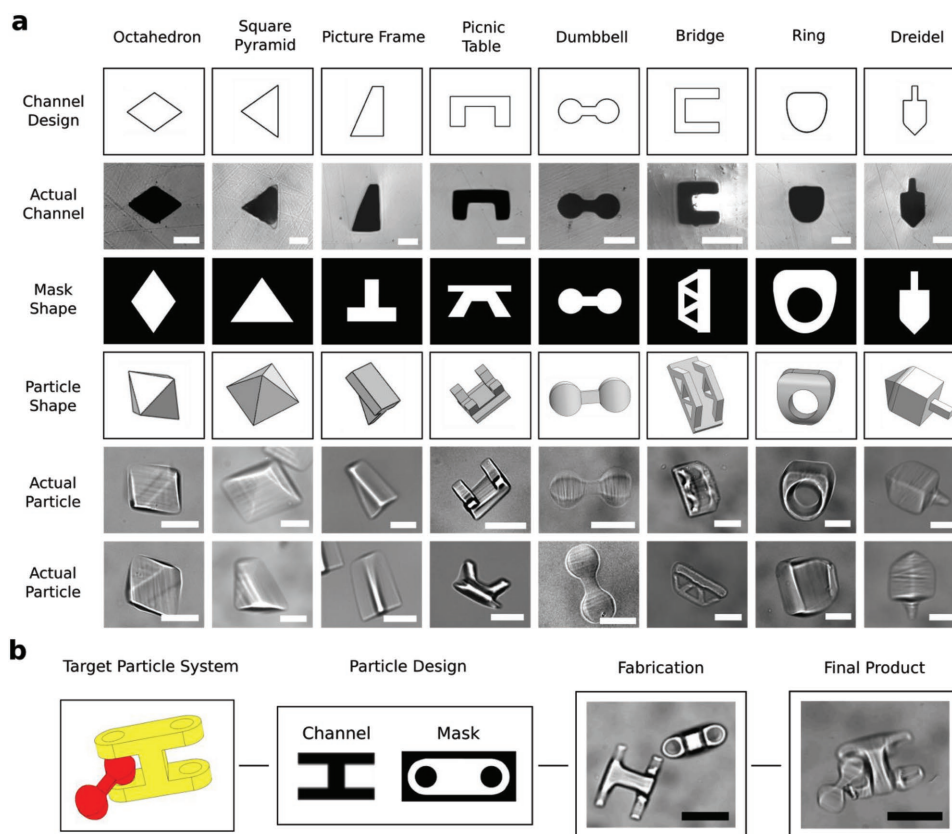
Figure 3. 3D microparticle design and fabrication. a) Eight types of particles designed and fabricated using the hollow fiber template from left to right: octahedron, square pyramid, picture frame, picnic table, dumbbell, bridge, ring, and dreidel. The grid displays, from top to bottom: the channel design, an image of the actual channel cross-section (scale bar 50 µm), mask shape, predicted particle shape, actual optical image of the particle (scale bar 50 µm), and an alternate angle of the actual particle (scale bar 50 µm). b) Design of multiparticle systems: a ball-and-socket connector for the dumbbell particle is designed and fabricated with good agreement between predicted and actual geometries (scale bars 100 µm).

branches by utilizing a dumbbell shaped channel with a lobed high-aspect ratio mask (Figure 4c).

In addition to the fabrication of hollow fiber templates with arbitrary cross-section, the thermal fiber drawing technique also enables integration of functional materials onto the channel surface. By codrawing a conductive polymer and cofeeding metal wires into the preform during the draw, it is possible to create arbitrarily placed conductive surfaces on the channel surface with low axial resistivity. Thus, highly tailorable external fields can be created within the hollow fiber template.

Here, we designed a hollow fiber template that is capable of spatially localizing microparticles randomly suspended in the prepolymer solution using dielectrophoretic (DEP) forces. DEP is an electrokinetic force induced on dielectric particles
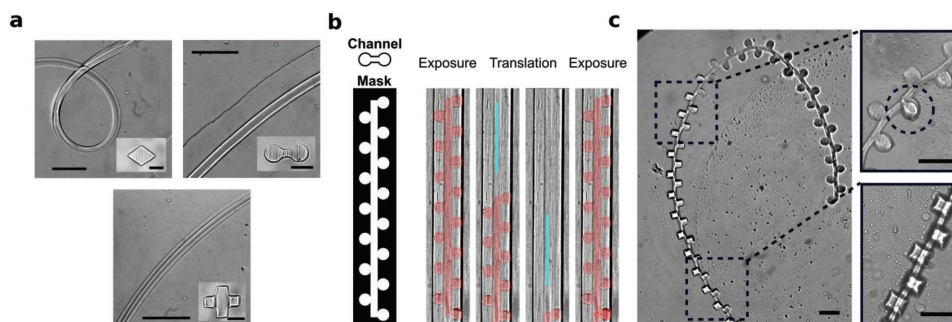

Figure 4. Microfiber fabrication. a) Continuous UV exposure of the hollow fiber template forms hydrogel fibers. We fabricated fibers with diamond, dumbbell, and cross shaped cross-sections (scale bar 300 µm, inset shows fiber cross-section with 50 µm scale bar). b) Exposure, translation, and exposure of high-aspect ratio masks can create axially asymmetric hydrogel fibers. c) A hydrogel fiber with alternating branched lobes was fabricated. (Top inset) Optical image of the lobe in which UV exposure was overlapped to connect two high-aspect ratio particles. (Bottom inset) Side view of the axially asymmetric fiber showing 3D geometric complexity. Scale bars represent 100 µm.

by nonuniform electric fields. For a homogeneous sphere of radius a and complex permittivity ε_p^* suspended in a media with complex permittivity ε_m^*, the time-averaged DEP force is

$$\langle F_{DEP} \rangle = 2\pi a^3 \varepsilon_m Re\left\{ \frac{\varepsilon_p^* - \varepsilon_m^*}{\varepsilon_p^* + 2\varepsilon_m^*} \right\} \nabla \left| \vec{E}_{rms} \right|^2 \quad (1)$$

Thus, the direction of the DEP force is determined by the sign of the $Re\left\{ \frac{\varepsilon_p^* - \varepsilon_m^*}{\varepsilon_p^* + 2\varepsilon_m^*} \right\}$ term, or the Clausius–Mossotti function (C–M factor), and the direction of the $\nabla \left| \vec{E}_{rms} \right|^2$ term. If the C–M factor is positive, the particles will migrate in the direction of increasing electric field gradient, or pDEP, and if it is negative, it will move in the opposite direction, called nDEP.

We designed a U-shaped channel within a COC cladding with its long vertical walls comprised of electrically conductive polyethylene (CPE). This preform design was then cofed with 50 µm copper wires to minimize its axial resistivity. The magnitude and direction of $\nabla \left| \vec{E}_{rms} \right|^2$ for our channel geometry were numerically simulated with an input voltage of 25 V and can be found in **Figure 5**a. The unique shape and electrode placement of the hollow fiber template creates DEP forces that will focus pDEP-feeling particles toward the interior corners of the channel, while nDEP particles will be focused to the channel corners located on the interior of the upper wall. We tested a 10 cm length of our DEP hollow fiber template by localizing 2 µm fluorescent polystyrene (PS) beads to the nDEP focusing positions. Because PS beads are well-known to exhibit nDEP behavior with a 10 MHz applied field in media with low electrical conductivity, the monomer solution was adjusted to contain only PEG-DA monomer, PEG, and 2-hydroxy-2-methylpropiophenone photoiniator.

In the absence of an electric field, the PS beads are distributed randomly throughout the hollow fiber template, and polymerization of hydrogel particles would not result in any bead localization. When a 50 V AC voltage is applied to the fiber at 10 MHz, the PS beads localize to the nDEP focusing positions predicted by the simulation (Figure 5b). At the polymerization step, we utilized a dumbbell shaped photomask that would result in a final particle shaped like two parallel pillars joined at the bottom by a rectangular connector with microbeads localized at the top interior corners (Figure 5c). The final fabricated particles were observed at multiple angles using a fluorescent microscope, and both their geometry and subparticle localization positions corresponded well to our predictions (Figure 5d). In addition, large area UV exposure enabled the fabrication of hydrogel fibers with localization of subparticles along the transverse axes (Figure 5e). It should be noted that some particles far from the particle focusing positions are not focused at the fiber outlet. This is due to the low DEP force at specific positions along the fiber cross-section relative to the rest of the channel. However, full particle migration can theoretically be achieved by either increasing the magnitude of the applied voltage or increasing the length of the fiber template to increase residence time.
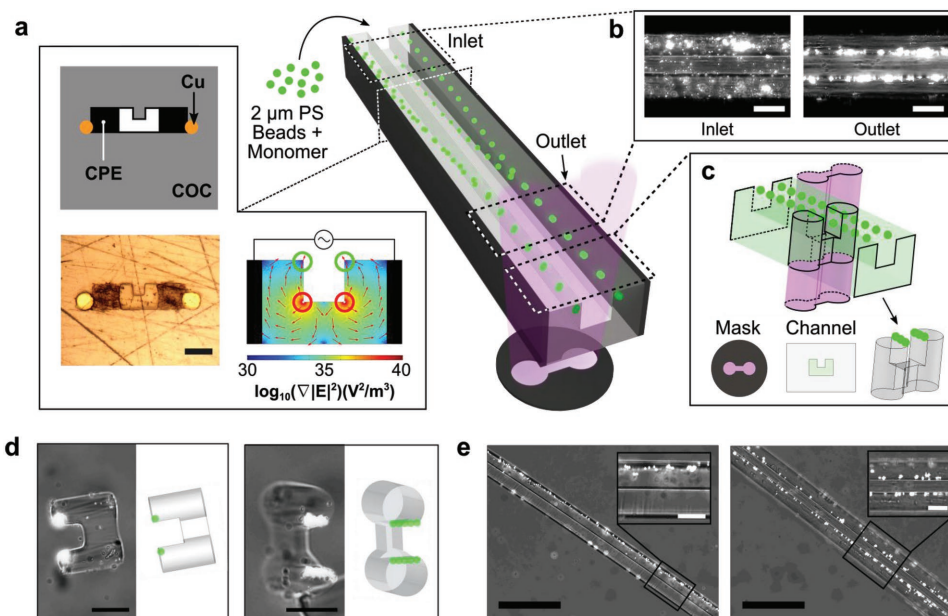

Figure 5. Subparticle localization using DEP. a) A schematic of the designed fiber cross-section (top) along with an optical image of the cross-section of a drawn fiber (bottom left) (scale bar 100 µm). A numerically simulated graph of the magnitude and direction of $\log(\nabla|E|^2)$ when a voltage differential of 25 V is applied to the electrodes (bottom right). Focusing positions for pDEP (red) and nDEP (green) guided particles are indicated with circles. b) Under no applied voltage, 2 µm PS particles within the DEP fiber are randomly distributed (left). Under 50 V at 10 MHz, particles focus to their nDEP focusing positions (right). Scale bars represent 50 µm. c) A dumbbell shaped masked was used to create a connected dual-pillared structure with subparticles (green) predicted to migrate to the interior edge of the pillars. d) Images of fabricated particles were taken under bright field and fluorescent light, demonstrating good agreement between predicted and actual microparticle geometry and fluorescent sub-particle (white) position (scale bar 50 µm). e) Hydrogel fibers showing subparticle localization along a side view (left) and top-down view (right). Scale bars represent 100 µm. Inset scale bars represent 30 µm.

**ADVANCED
SCIENCE NEWS**
www.advancedsciencenews.com

NANO · MICRO
small
www.small-journal.com

We present here a method for fabricating complex 3D hydrogel particles and fibers with feature sizes as small as 20 µm enabled by thermally drawn hollow fiber templates. In contrast to traditional microfabrication techniques, the hollow fiber templates can be structured with arbitrary cross-sectional shapes, allowing for biaxial control of microparticle and microfiber geometries. We are able to achieve improved geometric control because the factors determining the shape of each microobject (i.e., the channel structure and the photomask) were not affected by surface tension or flow-induced phenomena. These capabilities significantly expand the available range of producible microparticles and microfibers, such as the octahedrons, dreidels, diamond-shaped fibers, and axially asymmetric fibers we have demonstrated here. In addition, we utilized multimaterial fibers to produce tailored external fields within the hollow fiber template itself, allowing for subparticle localization within individual hydrogel particles using dielectrophoretic forces.

We would like to emphasize here that there exist several studies that utilize cross-sectional flow shaping and flow lithography to create complex 3D hydrogel particles[21–23,42] whose range of fabricable particle shapes is a subset of those included in our method. These approaches utilize hydrodynamic flow shaping of transient liquid molds, so fabricable particles have geometries limited to what can be realized through flow shaping, low throughput rates (12 particles min⁻¹), and limited flexibility in prepolymer composition. By contrast, our approach offers full design control of flow shaping in the flow direction, allowing for the synthesis of a much broader range of tailored particle shapes. In addition, we demonstrate order of magnitude improvement in fabrication throughput. Our approach also provides flexibility in prepolymer composition, which is critical in tailoring hydrogel pore size for functional applications such as DNA and RNA bioassays.[43]

While the minimum achievable feature size producible within a thermally drawn fiber has been shown to be as low as 600 nm[36] with no theoretical limitation to its overall geometry, limitations in the precision and resolution of our hydrogel microobject fabrication process prevent some conceivable structures from being readily realizable. First, although our materials selection process sought to reduce particle adhesion to the template surface by minimizing the surface energy of the cladding material, we found poor resolution of polymerized microshapes along sharp channel features on the scale of 20 µm and below. This indicates the possible presence of a thin inhibition layer at the polymer/fiber interface that does not polymerize during UV exposure, leading to reduced particle adhesion at the expense of geometric resolution. Previous studies of microfluidic particle fabrication in PDMS chips suggest that oxygen diffusion through porous PDMS walls leads to the presence of a thin, uncross-linked boundary layer at the PDMS/polymer interface with a thickness on the order of the oxygen penetration distance from the walls.[44] However, the oxygen permeability of our COC cladding is four orders of magnitude lower than that of PDMS, so it is unlikely that the same phenomenon is creating this inhibition layer. Thus, further studies on the mechanisms of particle formation within the hollow fiber template are needed to improve template resolution beyond the current threshold. An additional limitation is that the fiber

channel cross-section is axially symmetric and not dynamically changeable. That is, for every designed particle geometry, a new fiber must be fabricated. While this is not an issue when fabricating many particles of the same type and composition, creating fabrication devices with multiplexed components to create more compositionally complex microobjects would require external components (such as 3D printed chips) to link them together. We expect that this method of hydrogel microobject fabrication will have broad applications in next-generation biomaterials, such as self-assembled hydrogel particle scaffolds for tissue engineering or bone regeneration or hydrogel fibers that act as nerve scaffolds with microscale geometric features to aid in nerve cell alignment. The ability to subject the unpolymerized prepolymer solution to long-range external fields introduces additional functionality. For example, uniquely shaped particles with localized beads or magnetic particles could exhibit unique anisotropic mechanical properties or be effective anticounterfeit tools, while dielectrophoretic forces could be used to organize live cells within hydrogel fiber scaffolds to optimize their growth efficiency. In addition, an array of functional materials, such as piezoelectric materials, are compatible with the thermal drawing process, and could be used to induce alternative methods of particle migration, such as acoustophoresis. Ultimately, we demonstrate here a method that vastly expands the library of fabricable particles at high throughput, paving the way for a new generation of functional microobjects.

Experimental Section

Hollow Channel Fiber Fabrication: Aluminum rod template inserts with cross-sectional geometries similar to the desired channel shape were fabricated using wire electrical discharge machining. The aluminum rods were coated with a spray-on and heat-cured Teflon coating (Durafilm Teflon Black; applied by American Durafilm Co. Inc.).

Rectangular pockets were milled into two slabs of solid COC (TOPAS; grade 8007) such that the aluminum insert was completely enclosed within the preform. The excess void space between the aluminum template and the rectangular pockets was removed via annealing in a vacuum oven at 180 °C for 55 min. Following this consolidation step, the aluminum insert was removed to obtain the final preform.

The preforms were drawn into fibers using the thermal fiber drawing technique at 220 °C. The feed speed and draw down ratio were chosen such that channel size within the preform were reduced to the target dimensions. Fluidic connections were made to the fibers by inserting them into 0.004″ inner diameter PEEK tubing (IDEX Health and Science) and sealed with epoxy.

DEP Fiber Design and Fabrication: Simulation of the DEP force within a microfluidic channel with vertical wall electrode placement was performed using the electrostatics module in COMSOL. The shape and electrode placement along the channel were adjusted until particle equilibrium positions were localized to desired positions.

Slabs of COC, CPE, and Teflon were milled to shape, assembled, and consolidated in the same manner as above. Hollow channels that traversed the entire length of the preform were introduced in locations at which a channel or codrawn wire was to be placed.

Prior to the draw, the ends of a 50 µm copper wire spool were fed into fully traversing hollow channels within the preform. The spools were mounted atop a custom vertical spool holder that allowed the spool to unravel at low tension. The final preform assembly was then drawn in the manner as above.

3D Complex Microparticle Fabrication: Drawn fibers were interfaced by inserting the tip of the fiber into 0.004″ inner diameter PEEK tubing (IDEX Health and Science) and sealing with epoxy. The monomer

solution used in this work consisted of 31.5% (v/v) PEG-DA (molecular weight 700 g mol^{-1}), 18% (v/v) PEG (molecular weight 200 g mol^{-1}), 4.5% (v/v) Darocur 1173 (2-hydroxy-2-methylpropiophenone), and 1×Tris-EDTA buffer. Rhodamine B acrylate was added to the monomer solution at 5 µg mL^{-1} for the confocal experiments (Figure 2c), and 2 µm polystyrene beads were added at a concentration of 5.68 × 10^8 particles mL^{-1} (PolySciences), in the DEP study (Figure 5). Monomer solution was loaded into the tubing, and the tubing was connected to our in-house SFL setup as described previously.[17] Mylar photomasks (Fine Line Imaging) were designed in Autocad and placed in the field stop of the microscope (Zeiss Axio Observer A1). Compressed air was used to drive flow until the entire channel was filled with monomer solution. The flow was stopped, UV light was transmitted through the mask to polymerize a particle (exposure time between 100 and 200 ms), and the flow was restarted to flush the particle down the channel. This process was repeated using an automated Python script (Video S1, Supporting Information).

3D Complex Microfiber Fabrication: Drawn fibers were prepared as above and placed on top of our in-house contact lithography UV LED as described previously.[41] All components of the monomer solution were at the same concentration as above, and blue food coloring was added at 10% (v/v) to help visualize the stream. Monomer solution was loaded using a syringe until it filled the entire channel that was in contact with the UV LED. The syringe was manipulated until the flow stopped. UV light was transmitted through the drawn fiber template (exposure time between 1.5 and 2.0 s) to polymerize a hydrogel microfiber. The hydrogel microfiber was flushed out of the drawn fiber template and the process was repeated.

Axially asymmetric fibers were produced using projection lithography with high aspect ratio photomasks. Flow was stopped, and UV light was transmitted through the photomask to produce a short microfiber (≈700 µm). Flow was introduced slowly to push the short microfiber to the end of the field of view. UV light was transmitted again, overlapping the short microfiber to increase the length of the microfiber by ≈700 µm. This process was repeated until the fiber was sufficiently long.

Supporting Information

Supporting Information is available from the Wiley Online Library or from the author.

Acknowledgements

Conflict of Interest

The authors declare no conflict of interest.

[1] S. E. A. Gratton, P. A. Ropp, P. D. Pohlhaus, J. C. Luft, V. J. Madden, M. E. Napier, J. M. DeSimone, *Proc. Natl. Acad. Sci. USA* **2008**, *105*, 11613.

[2] J. A. Champion, S. Mitragotri, *Pharm. Res.* **2009**, *26*, 244.

[3] S. Barua, J. Yoo, P. Kolhar, A. Wakankar, Y. R. Gokarn, S. Mitragotri, *Proc. Natl. Acad. Sci. USA* **2013**, *110*, 3270.

[4] B. Das, A. Das, V. K. Kothari, R. Fanguiero, M. De Araújo, *Fibers Polym.* **2008**, *9*, 225.

[5] N. N. Shi, C.-C. Tsai, F. Camino, G. D. Bernard, N. Yu, R. Wehner, *Science* **2015**, *349*, 298.

[6] R. D. Farahani, K. Chizari, D. Therriault, *Nanoscale* **2014**, *6*, 10470.

[7] M. Mao, J. He, X. Li, B. Zhang, Q. Lei, Y. Liu, D. Li, *Micromachines* **2017**, *8*, 1.

[8] J. Xu, D. H. C. Wong, J. D. Byrne, K. Chen, C. Bowerman, J. M. Desimone, *Angew. Chem., Int. Ed.* **2013**, *52*, 6580.

[9] K. J. McHugh, T. D. Nguyen, A. R. Linehan, D. Yang, A. M. Behrens, S. Rose, Z. L. Tochka, S. Y. Tzeng, J. J. Norman, A. C. Anselmo, X. Xu, S. Tomasic, M. A. Taylor, J. Lu, R. Guarecuco, R. Langer, A. Jaklenec, *Science* **2017**, *357*, 1138.

[10] T. Nisisako, T. Ando, T. Hatsuzawa, *Small* **2014**, *10*, 5116.

[11] D. Dendukuri, K. Tsoi, T. A. Hatton, P. S. Doyle, *Langmuir* **2005**, *21*, 2113.

[12] A. R. Studart, H. C. Shum, D. A. Weitz, *J. Phys. Chem. B* **2009**, *113*, 3914.

[13] K. D. Seo, D. S. Kim, S. Sánchez, *Lab Chip* **2015**, *15*, 3622.

[14] W. Wang, X. H. He, M. J. Zhang, M. J. Tang, R. Xie, X. J. Ju, Z. Liu, L. Y. Chu, *Macromol. Rapid Commun.* **2017**, *38*, 1.

[15] L. Chen, H. Z. An, R. Haghgooie, A. T. Shank, J. M. Martel, M. Toner, P. S. Doyle, *Small* **2016**, *12*, 2001.

[16] D. Dendukuri, D. C. Pregibon, J. Collins, T. A. Hatton, P. S. Doyle, *Nat. Mater.* **2006**, *5*, 365.

[17] D. Dendukuri, S. S. Gu, D. C. Pregibon, T. A. Hatton, P. S. Doyle, *Lab Chip* **2007**, *7*, 818.

[18] P. Panda, K. P. Yuet, T. A. Hatton, P. S. Doyle, *Langmuir* **2009**, *25*, 5986.

[19] K. W. Bong, D. C. Pregibon, P. S. Doyle, *Lab Chip* **2009**, *9*, 863.

[20] J. H. Jang, D. Dendukuri, T. A. Hatton, E. L. Thomas, P. S. Doyle, *Angew. Chem., Int. Ed.* **2007**, *46*, 9027.

[21] K. S. Paulsen, D. Di Carlo, A. J. Chung, *Nat. Commun.* **2015**, *6*, 6976.

[22] C. Y. Wu, K. Owsley, D. Di Carlo, *Adv. Mater.* **2015**, *27*, 7970.

[23] K. S. Paulsen, Y. Deng, A. J. Chung, *Adv. Sci.* **2018**, *1800252*, 1.

[24] K. Choi, M. Salehizadeh, R. da Silva, N. Hakimi, E. Diller, D. K. Hwang, *Soft Matter* **2017**, *13*, 7255.

[25] N. Hakimi, S. S. H. Tsai, C. H. Cheng, D. K. Hwang, *Adv. Mater.* **2014**, *26*, 1393.

[26] J. P. Lata, F. Guo, J. Guo, P.-H. Huang, J. Yang, T. J. Huang, *Adv. Mater.* **2016**, *28*, 8632.

[27] E. Kang, G. S. Jeong, Y. Y. Choi, K. H. Lee, A. Khademhosseini, S.-H. Lee, *Nat. Mater.* **2011**, *10*, 877.

[28] H. Onoe, T. Okitsu, A. Itou, M. Kato-Negishi, R. Gojo, D. Kiriya, K. Sato, S. Miura, S. Iwanaga, K. Kuribayashi-Shigetomi, Y. T. Matsunaga, Y. Shimoyama, S. Takeuchi, *Nat. Mater.* **2013**, *12*, 584.

[29] S. Nakajima, R. Kawano, H. Onoe, *Soft Matter* **2017**, *13*, 3710.

[30] E. Kang, Y. Y. Choi, S. K. Chae, J. H. Moon, J. Y. Chang, S. H. Lee, *Adv. Mater.* **2012**, *24*, 4271.

[31] L. Leng, A. McAllister, B. Zhang, M. Radisic, A. Günther, *Adv. Mater.* **2012**, *24*, 3650.

[32] A. L. Thangawng, P. B. Howell Jr., C. M. Spillmann, J. Naciri, F. S. Ligler, *Lab Chip* **2011**, *11*, 1157.

[33] M. A. Daniele, K. Radom, F. S. Ligler, A. A. Adams, *RSC Adv.* **2014**, *4*, 23440.

[34] D. A. Boyd, A. R. Shields, P. B. Howell, F. S. Ligler, *Lab Chip* **2013**, *13*, 3105.

[35] A. L. Thangawng, P. B. Howell, J. J. Richards, J. S. Erickson, F. S. Ligler, *Lab Chip* **2009**, *9*, 3126.

[36] T. Khudiyev, C. Hou, A. M. Stolyarov, Y. Fink, *Adv. Mater.* **2017**, *29*, 1605868.

[37] B. Temelkuran, S. D. Hart, G. Benoit, J. D. Joannopoulos, Y. Fink, *Nature* **2002**, *420*, 650.

[38] A. Gumennik, A. M. Stolyarov, B. R. Schell, C. Hou, G. Lestoquoy, F. Sorin, W. McDaniel, A. Rose, J. D. Joannopoulos, Y. Fink, *Adv. Mater.* **2012**, *24*, 6005.

[39] S. Egusa, Z. Wang, N. Chocat, Z. M. Ruff, A. M. Stolyarov, D. Shemuly, F. Sorin, P. T. Rakich, J. D. Joannopoulos, Y. Fink, *Nat. Mater.* **2010**, *9*, 643.

[40] D. Dendukuri, S. S. Gu, D. C. Pregibon, T. A. Hatton, P. S. Doyle, *Lab Chip* **2007**, *7*, 818.

[41] G. C. Le Goff, J. Lee, A. Gupta, W. A. Hill, P. S. Doyle, *Adv. Sci.* **2015**, *2*, 1.

[42] K. S. Paulsen, A. J. Chung, *Lab Chip* **2016**, *16*, 2987.

[43] N. W. Choi, J. Kim, S. C. Chapin, T. Duong, E. Donohue, P. Pandey, W. Broom, W. A. Hill, P. S. Doyle, *Anal. Chem.* **2012**, *84*, 9370.

[44] D. Dendukuri, P. Panda, J. M. Kim, T. A. Hatton, P. S. Doyle, R. Haghgooie, *Macromolecules* **2008**, *41*, 8547.